The Six-Membered Intramolecular Hydrogen Bond Position as a Switch for Inducing an Excited State Intramolecular Proton Transfer (ESIPT) in Esters of *o*-Hydroxynaphthoic Acids

Javier Catalán,* Juan C. del Valle, José Palomar, Cristina Díaz, and José L. G. de Paz

Departamento de Química Física Aplicada, Universidad Autónoma de Madrid, Cantoblanco, E−28049 Madrid, Spain

Received: July 28, 1999; In Final Form: October 13, 1999

The substituted naphthalene compounds investigated in this paper, i.e., methyl 2-hydroxy-3-naphthoate (MHN23), methyl 1-hydroxy-2-naphthoate (MHN12), and methyl 2-hydroxy-1-naphthoate (MHN21), show a strong intramolecular hydrogen bond (IMHB) in their ground electronic state. The relative position of the IMHB in the naphthalene skeleton acts as a switch and controls the yield of an excited state intramolecular proton transfer (ESIPT) process. As a matter of fact, only MHN23 exhibits a proton transfer (PT) emission and possesses a theoretically proved ESIPT mechanism. The role that the ESIPT mechanism plays on the photostability of the molecule MHN23 is unravelled by comparison with the model compounds methyl salicylate (MS), MHN12, and MHN21. On one hand, the low photoreaction quantum yield, $\Phi_r = 0.00015$, and therefore the high photostability of MS, under direct ultraviolet (UV) irradiation, has been explained due to the photophysics of its proton transfer tautomer. On the other hand, (a) the two benzene-fused ring derivatives of methyl salicylate, MHN12 and MHN21, also possess a great photostability to UV radiation, and they do not support an ESIPT mechanism; and (b) although MHN23 exhibits an excited state proton transfer, its efficiency is only of 1.8%, and the photostability is 5 times larger than that of MS. As a result, the photostability of MHN23, MHN12, and MHN21 does not rely on the photophysics of their proton transfer tautomers but on the nonradiative dynamics of their respective normal tautomers. We present experimental evidence which supports the above-mentioned statement on the existence of distinctive nonradiative channels for the molecules MHN23, MHN12, and MHN21.

1. Introduction

The molecular skeleton of naphthalene exhibits two distinct nonequivalent carbon pair positions, 1−2 and 2−3, to which a six-membered intramolecular hydrogen bond (IMHB) ring can be linked. This special feature does not appear in benzene derivatives containing an IMHB ring, e.g., methyl salycilate (MS). For the benzene molecule, all the carbon pair positions are equivalent. This observation allows us to study the photophysical influence that the relative position of the intramolecular hydrogen bond ring has on the esters of *o*-hydroxynaphthoic acids, benzene-fused ring analogues of MS (Scheme 1). Thus, we aim at answering the following questions: does the IMHB position in the naphthalene ring influence the occurrence of an excited-state intramolecular proton transfer (ESIPT) process and how does the IMHB position affect the photostability of the molecule?

The molecules methyl 2-hydroxy-3-naphthoate (MHN23) and methyl salicylate possess a strong IMHB in the ground electronic state and yield a proton transfer emission with a low quantum yield.[1,2] In accordance with the general belief[3−9] found in the references, the great photostability shown (cf. Photostability section) by MHN23 and MS relies on the photophysics of their proton transfer tautomers (PT-tautomer, Scheme 2). On the other hand, the molecules methyl 1-hydroxy-2-naphthoate (MHN12) and methyl 2-hydroxy-1-naphthoate (MHN21) also present a strong IMHB, but they do not undergo an ESIPT mechanism, however, exhibit a high photostability to ultraviolet irradiation (vide infra). How could we explain this seeming controversy? Thus, we aim at understanding the relationship which links the photostability of intramolecular hydrogen bonded aromatic molecules to an ESIPT mechanism.

Evidence on the existence of the intramolecular hydrogen bonded MHN23 molecule has already been reported by Bergmann et al.[12] The observation of a dual emission in the fluorescence spectrum of MHN23 was first established by Naboikin et al.[13] Those emissions are a short-wavelength fluorescence at ca. 410 nm and a long-wavelength emission (exhibiting approximately a 10 000 cm^{-1} shift from the first absorption band), of the type described by Weller[14−16] for methyl salicylate, at ca. 650 nm. The long-wavelength emission was ascribed to the effects of the intramolecular hydrogen bond of the molecule MHN23. Naboikin et al.[13] ruled out the possibilities of rationalizing the 650 nm emission band as it being produced by dimer or excimer species. Finally, Woolfe and Thistlethwaite[1] ascribed the long-wavelength fluorescence to the excited state proton transfer tautomer of MHN23 (PT-tautomer, Scheme 2). Nevertheless, they placed the PT-tautomer fluorescence at 608 nm, which is not consistent with the results reported by Naboikin et al.[13] Our results show (vide infra) that, when the emission spectrum is corrected for instrumental sensitivity, the wavelength maximum shifts to ca. 650 nm, thereby matching the wavelength value found by Naboikin et al.[13]

* To whom correspondence should be addressed. Fax: 34 91 397 4187. E-mail: javier.catalan@uam.es.

10.1021/jp992631p CCC: $18.00
Published on Web 11/25/1999

SCHEME 1

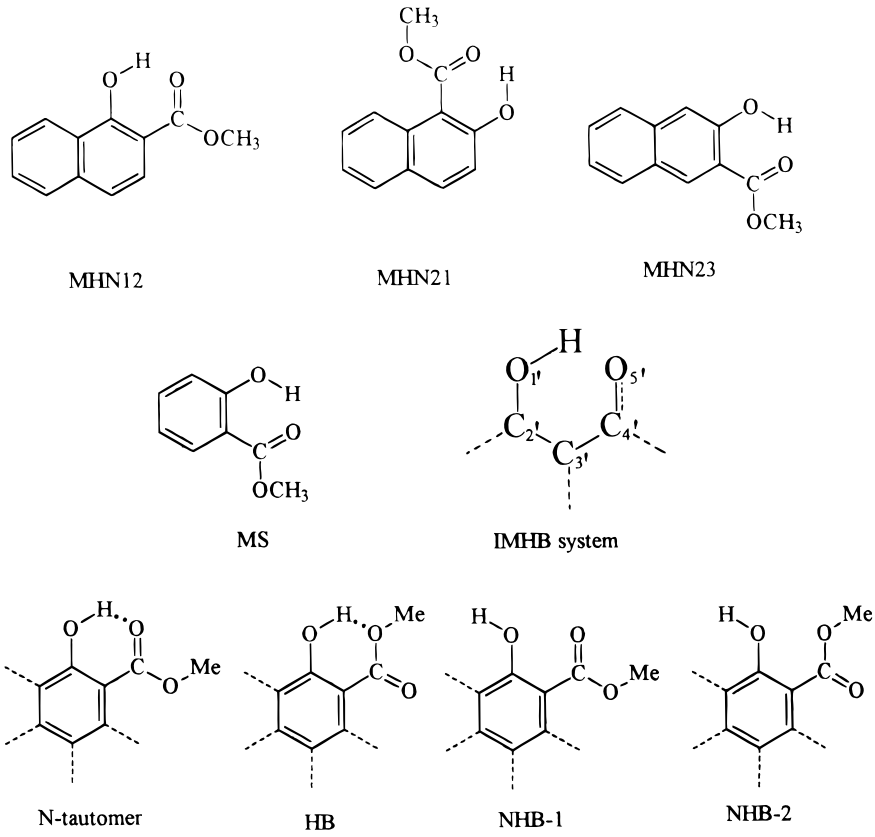

SCHEME 2

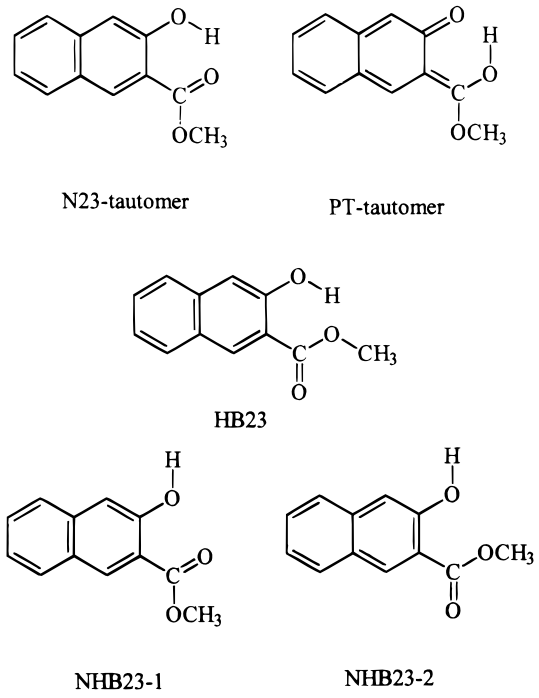

According to Woolfe and Thistlethwaite[1] the commonly observed MHN23 fluorescence at ca. 410 nm exhibits a distinct excitation spectrum compared to that of the long-wavelength band, and neither resembles the UV absorption spectrum.[1] We show in this paper discrepancies with those results, because after correcting the excitation spectra for instrumental sensitivity, the excitation spectrum of the long-wavelength band definitely matches the absorption spectrum. Thus, only one of the corresponding isomers, the N23-tautomer species, is predominant in the ground electronic state. The observation of only one predominant isomer for the ground state is also common to methyl salicylate and the salicylic acid family.[17] Thus, we give emphasis to the correction of the emission and excitation spectra to acquiring a better understanding of the photophysical phenomena.

Also, Woolfe and Thistlethwaite[1] suggested that two ground state conformers (Scheme 2, HB23 and NHB23-1) must exist in order to explain the finding of a dual exponential decay time for the short-wavelength emission band in cyclohexane and methanol solutions.

Methyl salicylate and its naphthalene derivative MHN23 have recently drawn attention[10,11] to interpreting the photophysical behavior and ground state concealed isomers of methyl salicylate. Furthermore, the molecule salicylic acid and many of its derivatives have been reported for being tribo-active materials very useful in dry xerographic toners.[10,18−22]

In addition, the photophysics of MHN12 and MHN21 has received little interest in the literature; therefore, we are presenting a thorough photophysical study of these molecules in both cyclohexane solution and the gas phase.

For the first time, the photophysical influence of the IMHB position in an aromatic molecule has been studied theoretically (by means of hybrid density functional theory) and experimentally. From this information, we unravel the important role that the IMHB ring position plays in the excited state intramolecular proton transfer for esthers of the *o*-hydroxynaphthoic acids.

2. Experimental Section

Instrumentation. The absorption spectra for liquid samples at 298 K were monitored on a Shimadzu UV-2100 spectrometer using Suprasil cells of a 1 cm path length. The gas-phase

absorption spectra at 353 K were obtained with the aid of a Cary 5 spectrometer using Suprasil cells of a 10 cm path length at 353 K.

Emission and excitation measurements were carried out on an SLM Aminco-Bowman series 2 luminescence spectrometer at the temperatures shown in the text or figure captions.

The gas-phase emission spectra were recorded for samples obtained by sublimating the compounds (MHN12, MHN21, and MHN23) in a closed cell (1 cm path length) through which a stream of 99.999% pure N_2 was circulated for 30 min (prior to the heating of the sample). All of the emission and excitation spectra shown in this paper have been appropriately corrected for instrumental sensitivity. The emission spectra were corrected using as a standard a lamp of spectral irradiance (Optronic Laboratories, Inc., OL 245 M).

Degassed samples were prepared with the aid of a vacuum pump to 4×10^{-5} mbar using five freeze−pump−thaw cycles.

Quantum yields were calculated with the aid of the above-mentioned instrument (SLM Aminco-Bowman) at 298 K on freshly prepared samples with absorbances at the excitation wavelength (293 nm) of ca. 0.05. The sample 2-aminopyridine in 0.1 N H_2SO_4 was employed as a standard ($\Phi_f = 0.66$) to measure the fluorescence quantum yields, which were corrected taking into account the refractive indices of the solvents used.

Fluorescence lifetimes were determined with phase and modulation measurements, relative to glycogen scattering solutions by using an SLM 48000S spectrofluorimeter at frequencies between 1 and 250 MHz. Decisions on the suitability of the lifetimes rested on examination of the statistics of a fit (a plot of the residual deviations with frequency) and the reduced χ^2 values. In our experiments, the reduced χ^2 values were all close to unity. The detection limit of our intrument is ca. 30 ps.

Photostability at 298 K was determined by using a PTI system, consisting of a horizontally mounted water-cooled lamp housing for a 1000 W xenon lamp furnished with an *f*/4.0 elliptical reflector that concentrated the lamp intensity 4-fold. Light reflected to the sample chamber was previously passed through a water-cooled PTI 02-A002 infrared water filter and then through a monochromator by which a wavelength was selected for sample excitation. The photon flux reaching the sample was measured with the Aberchrome 540.[38] The samples used were stirred continuously during the irradiation. Sample degradation was monitored by UV spectroscopy on a Shimadzu UV-2100 spectrometer and was expressed by means of the quantum yield of photoreaction (Φ_r) as the ratio between the number of moles converted or photodegradated and the einsteins (moles of photons) absorbed by the sample at the excitation wavelength (340 nm for MHN12 and MHN21, 368 nm for MHN23, and 308 nm for MS). All the photolysis experiments were carried out in cyclohexane. None of the samples show aggregation or non-Beer−Lambert behavior at the concentrations used. The photoreaction quantum yields were appropriately corrected taking into account the respective fluorescence quantum yield of the compounds studied.

The infrared (IR) data for the molecules MHN12, MHN21, and MHN23 within the range 4000−450 cm^{-1} were recorded on a Fourier transform Nicolet Impact 410 spectrometer at room temperature with 200 scans and 1 cm^{-1} in resolution. The IR spectra were recorded in CCl_4 and cyclohexane solutions.

Theoretical Calculations. Hybrid density functional methods have been applied to several studies of molecular systems containing an intramolecular hydrogen bond. These methods predict molecular data that match the available experimental ones, as well as the results obtained with the highest post-HF methods.[39−42]

Geometry optimization and vibrational data for the structures studied in this paper were computed at B3LYP[43,44] level using the 6-31G** basis set. For the sake of comparison between experimental and calculated IR spectra, the calculated wavenumber values have been drawn to scale by multiplying by 0.9613.[45]

The evaluation of potential energy surfaces (PES) that describe the proton motion entails a molecular structure optimization.[46] Ground state intramolecular proton transfer curves (GSIPT) were calculated with the energies of the B3LYP/6-31G** fully optimized structures at fixed O−H distances over the 0.9−1.6 Å range.

Information on the ESIPT mechanism was obtained by calculating the Franck−Condon transition energies for the B3LYP/6-31G** ground state structures at the CIS/6-31G** level.[47] The Franck−Condon curves for the proton transfer process were obtained by adding the CIS/6-31G** excitation energies to the corresponding GSIPT curves. This modeling, which does not include excited state optimization, has been successfully applied to the ESIPT study of hydroxybenzoyl compounds and displays a good agreement with the photophysical evidence.[48]

An energy increment value E_{PT} is used for evaluating the occurrence of the proton transfer process in the ground state. This energy increment for the $S_0' \rightarrow S_0$ back proton transfer process is regarded as the difference between the energy at the equilibrium distance of the N-tautomer and the energy of the PT-tautomer at $r_{OBH} = 1.6$ Å

The strength of the intramolecular hydrogen bond (IMHB) was estimated as the difference (E_{IMHB}) between the energy of the fully optimized molecular structures of the non-hydrogen-bonded form (with a hydroxy group rotated 180°, i.e., NHB-1 in Scheme 1) and the energy of the N-tautomer molecule.

All the calculations have been performed with the Gaussian 94 program.[49]

Synthesis. Methyl 2-hydroxy-3-naphthoate (MHN23) was purified by silica gel column chromatography using *n*-hexane/ethyl acetate (1:1) as eluent. Methyl 1-hydroxy-2-naphthoate (MHN12) and methyl 2-hydroxy-1-naphthoate (MHN21) were obtained by refluxing for 1 day the corresponding acids with methyl alcohol in the presence of sulfuric acid. Finally, MHN12 and MHN21 were purified by silica gel column chromatography using *n*-hexane/ethyl acetate (80:20) and *n*-hexane/dichloromethane (80:20) as eluents, respectively.

3. Hydrogen Bond Strength and Stability of the Rotamers

The theoretical stabilities (Table 1) indicate that the S_0 state intramolecular hydrogen bond of both molecules MHN12 and MHN21 is stronger than that of methyl salicylate (MS). In contrast, MS has a stronger S_0 hydrogen bond than that of MHN23. That fact is clearly developed by observing the calculated distances of the six-membered IMHB ring of the N-tautomers of these compounds (Table 2). Thus, a more effective hydrogen bridge lengthens the $O_{1'}$−H bond distance (Scheme 1) and shortens the $O_{1'}\cdots O_{5'}$ and $H\cdots O_{5'}$ distances of the MHN12 and MHN21 compounds with respect to those of MS; while the converse distance variations apply to the MHN23 molecule. As can be seen in Table 2, there exists a resonance-assisted hydrogen bond mechanism[50] that produces the shortening of the $C_{2'}-O_{1'}$ and $C_{3'}-C_{4'}$ distances (increased double bond character) and the lengthening of the $C_{4'}-O_{5'}$ and $C_{2'}-C_{3'}$ distances (decreased double bond character). Thus, the proton

TABLE 1: Calculated Energy Values (in kcal/mol) at the B3LYP/6-31G Level: IMHB Strength (E_{IMHB}); Electronic Energy Increments between the N-Tautomer and Both the HB ($\Delta E_{HB-(N-tautomer)}$) and the NHB ($\Delta E_{NHB-(N-tautomer)}$) Species; Free Energy Increment between the N-Tautomer and the HB Species ($\Delta G_{HB-(N-tautomer)}$); Energy Difference ($E_{PT}$) between the N-Tautomer (at the Equilibrium Distance) and the PT-Tautomer at a R_{O-H} Distance of 1.6 Å**

	$E_{IMHB}/\Delta E_{NHB-1-N-tautomer}$	$\Delta E_{HB-N-tautomer}$	$\Delta G_{HB-N-tautomer}$	$\Delta E_{NHB-2-N-tautomer}$	E_{PT}
MHN21	15.6	3.4	2.8	13.3	13.1
MHN12	15.4	4.3	4.1	14.7	13.0
MS	12.3	3.8	3.6	11.7	17.6
MHN23	11.5	3.7	3.2	10.7	21.5

TABLE 2: Calculated Bond Distances (in Å) at the B3LYP/6-31G Level for the Intramolecular Hydrogen Bond Ring (cf. Scheme 1) of the N-Tautomer (at the Equilibrium Distance) and PT-Tautomer (R_{O-H} = 1.6 D)'**

	MHN21	MHN12	MS	MHN23
Normal Tautomer Bond Distances				
O1′−H	0.997	0.992	0.987	0.985
O1′−C2′	1.334	1.338	1.342	1.346
C2′−C3′	1.415	1.405	1.42	1.439
C3′−C4′	1.471	1.464	1.469	1.473
C4′−O5′	1.240	1.237	1.234	1.232
O5′···H	1.591	1.679	1.72	1.73
O1′···O5′	2.497	2.576	2.606	2.614
Proton-Transfer Tautomer Bond Distances				
O1′···H	1.600	1.600	1.600	1.600
O1′−C2′	1.266	1.267	1.272	1.278
C2′−C3′	1.467	1.452	1.462	1.473
C3′−C4′	1.408	1.402	1.408	1.417
C4′−O5′	1.310	1.308	1.303	1.297
O5′−H	1.014	1.021	1.027	1.032
O1′..O5′	2.521	2.536	2.543	2.548

TABLE 3: Theoretical and Experimental Carbonyl and Hydroxyl Stretching Frequency Values (in cm^{-1}) for the N-Tautomer and HB Species

	$\nu(C{=}O)_{exp}$	$\nu(C{=}O)_{theor}$	$\nu(O-H)_{exp}$	$\nu(O-H)_{theor}$
N21-tautomer	1654	1642		3163
HB21	1728	1719	3369	3434
N12-tautomer	1670	1658		3178
HB12	1730	1734	3397	3468
$MS_{N-tautomer}$	1682	1672	3196	3274
MS_{HB}	1731	1735	3450	3506
N23-tautomer	1690	1678	3255	3319
HB-23	1736	1737	3481	3526

donor and acceptor groups are connected by a π-conjugated double-bond system, whose principal effect is to make the homonuclear IMHB stronger.[50] By using infrared spectroscopy, Hurnsberger[51,52] also drew the same conclusions.

The theoretical IR frequency values for the hydrogen bonded N-tautomers resemble quite well the experimental IR spectra in cyclohexane and CCl_4 solutions. Table 3 illustrates the excellent equivalence between the experimental IR carbonyl and hydroxyl stretching frequencies and the respective theoretical frequencies.

In assigning the molecular structures for the ground electronic state (Schemes 1−3), we take into account the C═O and O−H stretching frequencies (Table 3). Thus, the frequencies ν(C═O) (experimental data) and ν(O−H) (theoretical data) appear shifted to the red compared to those of the model compounds 1-methylnaphthoate ($\nu_{C=O}$ = 1724 cm^{-1}),[50] 2-methylnaphthoate ($\nu_{C=O}$ = 1726 cm^{-1}),[50] 1-naphthol (ν_{O-H} = 3606 cm^{-1}), and 2-naphthol (ν_{O-H} = 3607 cm^{-1}). The carbonyl frequency shift increments of 82 cm^{-1} for MHN21, 62 cm^{-1} for MHN12, and 48 cm^{-1} for MHN23, referred to the model compounds, indicate the presence of strong intramolecular hydrogen bonds (in sequence of decreasing strength), which according to Zadorozhnyi[53] correspond to energy stabilities (E_{IMHB}) of 10.2, 8.1, and 5.2 kcal/mol, respectively.

SCHEME 3

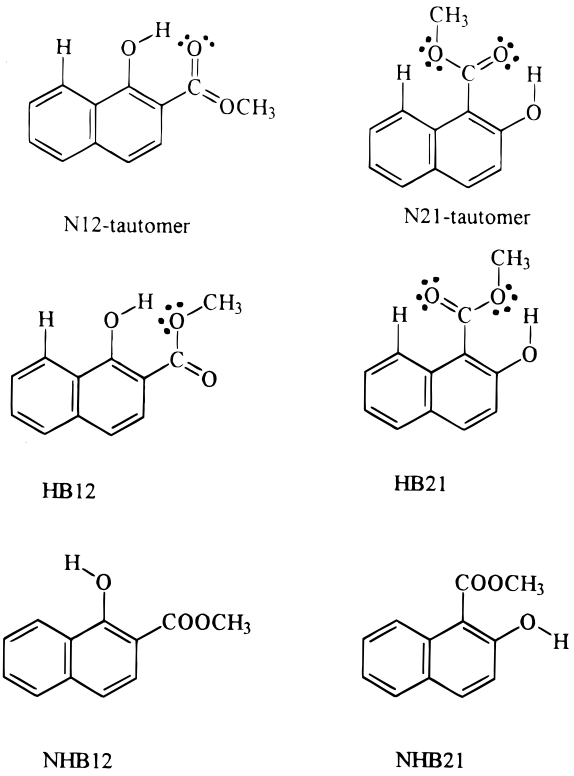

Table 1 gathers the energy stabilities of the different rotamers of MHN12, MHN21, and MHN23. Their relative stability reveals that the ground-state equilibria *N-tautomer (or HB)* ⇌ *NHB* (Scheme 1) should be shifted in favor of the species containing an intramolecular hydrogen bond. The theoretical free energies (Table 1) calculated at the B3LYP/6-31G** level include electronic energies, unscaled zero-point energies, enthalpy temperature corrections, and absolute entropies at 298.15 K and 1 atm, derived by using the calculated harmonic vibrational frequencies and the standard statistical thermodynamic relationships. Thus, from the calculated free energies we can estimate the equilibrium constants corresponding to the different rotamers. For the ground state equilibrium *N-tautomer* ⇌ *HB*, the equilibrium constants are as follow: 9.0 × 10^{-3} (MHN21); 1.0 × 10^{-3} (MHN12); 4.0 × 10^{-3} (MHN23). The S_0 chemical equilibria clearly lie in favor of the N-tautomer species. On the basis of those equilibrium constants, the population ratios in the gas phase for the N-tautomer vs HB are ca. 111:1 for MHN21, 1000:1 for MHN12, and 250:1 for MHN23.

For the above-mentioned molecules, the IR spectra in CCl_4 and cyclohexane solutions show a weak absorption band at ca. 1730 cm^{-1}, which is also found for the molecule MS and was tentatively assigned by Toribio et al.[54] to the free carbonyl stretching band of the HB isomer. Furthermore, our IR spectra indicate a small shoulder at ca. 3400 cm^{-1} that may be assignable to the O−H stretching frequency of the naphthol

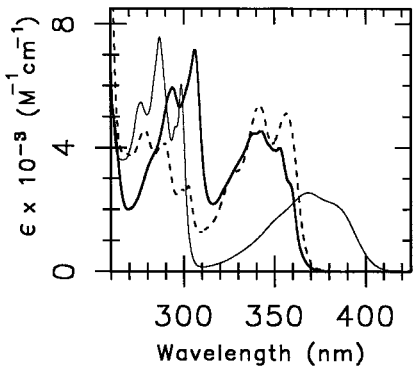

Figure 1. Absorption spectra of the molecules MHN12 (dash line), MHN21 (thick solid line), and MHN23 (thin solid line) in cyclohexane solution at 298 K.

group, thus weakly bonded to the ether oxygen of the adjacent ester susbtituent by means of an IMHB.[54] It is noteworthy that the wavenumber position and the intensity ratio of the IR bands mentioned above do not depend on concentration and agree with the calculated IR peaks of the respective rotamers (Table 2). However, it is theoretically proved for methyl salicylate that the frequencies for the free carbonyl groups of the rotamers HB and NHB are almost identical. To check the assignment of the free carbonyl frequency, the basicity of the solvent used was increased, and thus an enhancement of the free carbonyl (1730 cm^{-1}) and the hydroxy (3400 cm^{-1}) stretching band intensities was monitored. This latter fact denotes that the hydroxy group is intermolecularly bonded to a nucleophilic heteroatom of the solvent, thereby forming NHB species. Therefore, we also attribute the frequency localized at 1730 cm^{-1} to the free carbonyl group.

On the other hand, from the theoretical IR intensities of the carbonyl frequencies of the N-tautomers and HB species, in conjunction with the baseline corrected experimental absorbances of the 1730 cm^{-1} and 1650−1690 cm^{-1} bands in cyclohexane solution (Table 3), the relative presence of the molecules N-tautomer vs HB is estimated to be 23:1 for MHN21, 96:1 for MHN12, and 66:1 for MHN23. These molecular ratios are consistent with the theoretically predicted stability of the rotamers, thereby showing that the HB isomer of MHN21 is especially stabilized compared to that of MHN12. This stabilization is due to the *peri effect*[30,32] of the hydrogen atom at position 8 (H-8) that effectively favors the twisting of the esther group, because of the formation of a hydrogen bond between the oxygen of the carbonyl group and the H-8 atom.

In summary, the theoretical and experimental IR data show strong IMHBs, for the N-tautomer species, whose stabilization energies are on the decrease for the following molecular sequence MHN21, MHN12, and MHN23. The theoretical equilibrium constants estimated predict that the N-tautomers are also the main absorbing species in the S_0 state, in accord with the IR data in CCl_4 and cyclohexane solutions.

4. Absorption in Cyclohexane Solution

The absorption spectra of the molecules MHN12, MHN21, and MHN23 in hydrocarbon solution are depicted in Figure 1. As can be seen, the first absorption bands of the molecules MHN12 and MHN21 are placed at approximately the same wavelength region. However the first absorption band of MHN23 is red shifted ca. 40 nm compared to the absorption bands of MHN12 and MHN21. This is also consistent with the theoretical $S_0 \rightarrow S_1$ electronic energies gathered in Table 4. This fact can be accounted for by the electronic modification that

TABLE 4: Electronic Energies (cm^{-1}) and Oscillator Strength Values of the First Excited Electronic Transition Obtained at the CIS/6-31G//B3LYP/6-31G** Level**

	MHN21		MHN12		MHN23	
	energy	*f*	energy	*f*	energy	*f*
S_1 N-tautomer	40 334	0.21	39 827	0.18	37 728	0.12
S_1 PT-tautomer					29 155	0.20
S_1 HB	40 649	0.18	40 220	0.17	38 363	0.11
S_1 NHB-1	40 396	0.19	40 267	0.14	39 774	0.09
S_1 NHB-2					39 602	0.08

the six-membered IMHB ring (linked at the 1−2 or 2−3 positions) produces on the naphthalene system. As a matter of fact, the first absorption band of anthracene ($S_0 \rightarrow S_1$ band maximum at 374.5 nm) is definitely 44.5 nm red shifted compared to the first absorption band ($S_0 \rightarrow S_1$ band maximum at 330 nm) of phenanthrene in *n*-hexane solution.[55] In accordance with Platt's theory[55,56] (Scheme 4) the lowest excited state transition is polarized in the short molecular axes for anthracene (^1L_a) and for phenanthrene (^1L_b). Thus, by taking into account our theoretical calculations, for MHN23 the transition dipole moment of the S_1 state is located in the short molecular axis (being ^1L_a as the one for anthracene) and the S_1 transition dipole moments for MHN12 and MHN21 are forming an angle of 33.9°, and 15.3°, respectively, referring to the ^1L_b axis of phenanthrene (Scheme 4). Thus, as an analogy of the MHN21 and MHN12 molecules with phenanthrene and of MHN23 with anthracene, a predominant intramolecular hydrogen-bonded molecular structure (N-tautomer, Scheme 1) is expected in hydrocarbon solution and the gas phase (cf. section 3). Also, from the large absorption coefficient values, it is clear that the first electronic transition is π,π^* in nature for all the compounds.

5. Emission in Cyclohexane Solution

Figures 2a and 3a depict the absorption and emission spectra of the molecules MHN12 and MHN21, respectively. As observed, the corresponding absorption and emission bands do not show a very good mirror image symmetry, in part because the absorption band half-width is 1400 and 1000 cm^{-1} smaller than the emission band half width for the molecules MHN12 and MHN21, respectively. However, the bandwidth anomalies may imply that (a) other chemical structures can be contributing to broaden the emission band of the two compounds above or (b) the S_1 potential surface minimum suffers a major displacement from the S_0 potential surface minimum, and thus a skeletal distortion of the excited molecule is produced with a consequent broadening of the emission band. As is shown in Figures 2b and 3b, the excitation spectra of the respective emission bands match the absorption spectra quite well. Thus, the emission spectra come predominantly from the absorption spectra corresponding to mainly one of the chemical structures. Furthermore, for the reason that the excitation spectra obtained by monitoring the whole range of the emission band resemble each other, as well as the respective absorption spectra of MHN12 and MHN21, explanation (a) should be discarded. As a result, the evident failure of Levshin's law is explained by a displacement between both potential energy curve minima of the S_1 and S_o states.

The fluorescence quantum yields of the compounds MHN12 and MHN21 in cyclohexane are 0.19 and 0.04, respectively (on excitation at 293 nm). No evidence of proton transfer emission was monitored in the course of the experiments at dilute solutions, neither at very concentrated solution nor at the crystal phase for the MHN12 and MHN21 molecules. Recently, Tobita et al.[11] have reported the absence of the ESIPT mechanism in

SCHEME 4: S_1 Transition Dipole Moments for the Molecules MHN12 (μ_{12}), MHN21 (μ_{21}), and MHN23 (μ_{23}) Oriented (α, β, γ) with Respect to the S_1 Transition Dipole Moments (L_a, L_b) of Phenanthrene and Anthracene[a]

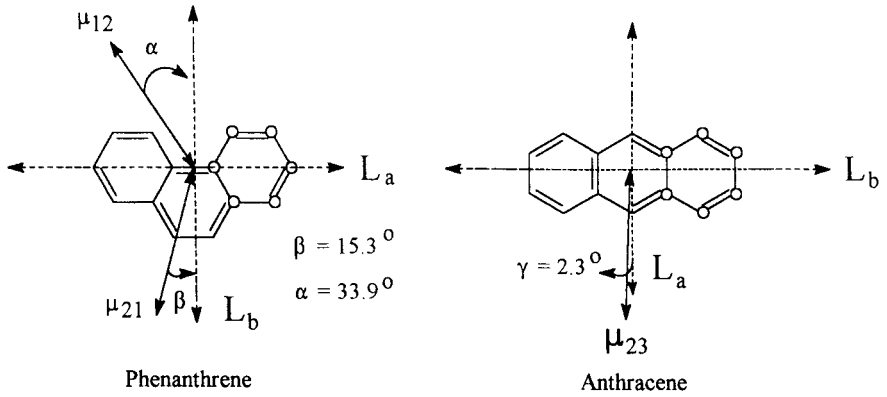

[a] IMHB ring position is indicated with hollow circles.

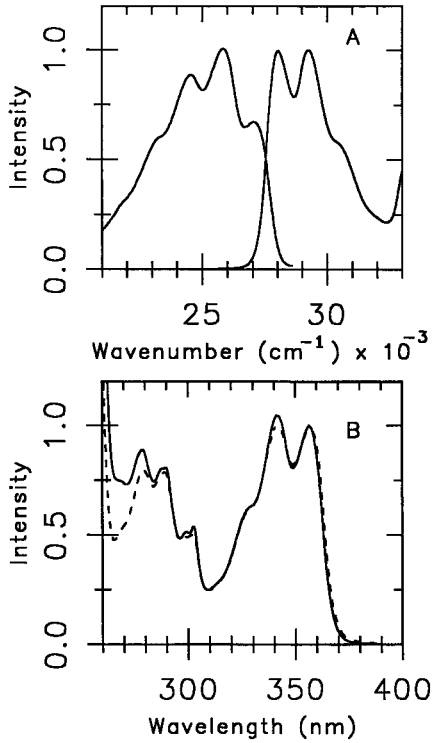

Figure 2. (A) Absorption (right) and fluorescence (left) spectra of MHN12. (B) Absorption (solid line) and excitation (dash line) spectra of MHN12. The experiments were carried out in cyclohexane at 298 K.

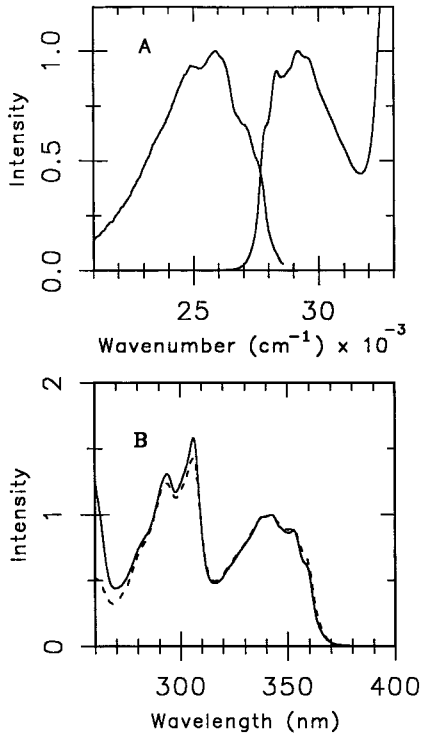

Figure 3. (A) Absorption (right) and fluorescence (left) spectra of MHN21. (B) Absorption (solid line) and excitation (dash line) spectra of MHN21. The spectra were recorded at 298 K in cyclohexane solution.

the molecule MHN12 by means of transient absorption in the ground state, fluorometry, and time-resolved thermal lensing (TRTL) measurements.

The MHN23 molecule exhibits two fluorescences (Figure 4) in cyclohexane solution with peaks at 400 nm and at ca. 650 nm and fluorescence quantum yields of 0.003 (this paper) and 0.0007,[32] respectively. On one hand, the 650 nm fluorescence ascribed to the PT-tautomer possesses an excitation spectrum which resembles the MHN23 absorption spectrum (Figure 5). On the other hand, the excitation spectrum of the short-wavelength fluorescence is blue shifted with respect to the absorption spectrum (Figure 5). This latter excitation spectrum was recorded at different emission wavelengths from 390 to 500 nm without showing any significant difference in profile. HB23, NHB23-1 and NHB23-2 (Scheme 2) could seemingly account for the 410 nm emission band. In fact, since the excitation spectra of the 650 nm emission band match the absorption spectra, the N-tautomer population in the ground state must be present in a much larger contribution than that of HB23, NHB23-1, and NHB23-2.

6. Lifetimes in Cyclohexane Solution

For MHN12 on excitation at 335 nm, the lifetime modeling fits a decay time of 2.2 ns with a fractional contribution of 85% and a second decay time of 0.7 ns. On excitation at 350 nm, the same decay times are found but the fractional contribution of the 2.2 ns decay time is 95%. From the theoretical calculations (cf. section 3), a free energy of 4.1 kcal/mol is predicted for the reaction *N12-tautomer* $\rightleftharpoons$ *HB12*. Both molecules are in thermodynamic equilibrium in the ground state with an equilibrium constant of 1.0×10^{-3}, which indicates that the equilibrium should be almost entirely in favor of N12-tautomer. Therefore, the absorption spectrum would bear a close similarity to the excitation spectra, as is observed in Figure 2b.

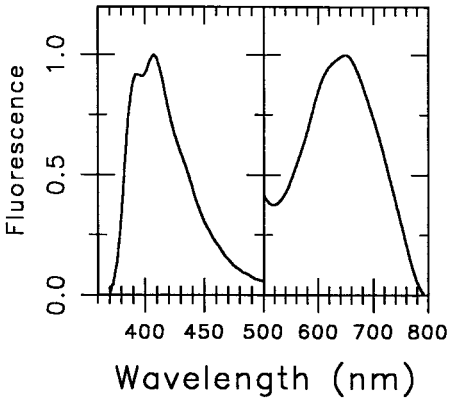

Figure 4. Dual fluorescence of MHN23 in cyclohexane at 298 K: (left) short wavelength band; (right) proton transfer emission.

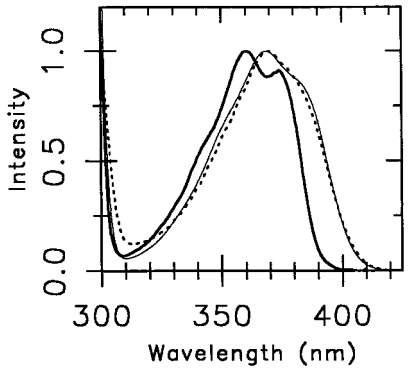

Figure 5. Absorption spectrum (thin solid line), excitation spectrum from the proton transfer emission (dash line), and excitation spectrum from the short-wavelength emission (thick solid line) of the molecule MHN23. All the experiments were measured in cyclohexane at 298 K.

In contrast, a very small equilibrium constant ($k = 5.1 \times 10^{-12}$) is estimated from the electronic energy for the equilibrium *N12-tautomer* ⇌ *NHB12-1* (Table 1); thus, the contribution in cyclohexane solution of NHB12-1 to the ground state population should be neglected. As a result, since the excitation spectra of the MHN12 fluorescence matches the absorption spectra and the IR estimated ratio of the two feasible conformers, i.e., N12-tautomer and HB12, is 96:1, respectively, the longer decay time of 2.2 ns is assigned to the N12-tautomer and the shorter one to the HB12 species. This interpretation is also supported by the consistency between the radiative constants calculated from both the absorption spectrum of MHN12 ($K_r = 4.3 \times 10^7$ s^{-1}) (according to the Strickler and Berg's equation)[57] and the ratio between the fluorescence quantum yield and the lifetime ($\tau_f =$ 2.2 ns) of the N12-tautomer, $K_f = \Phi_f/\tau_f$ (8.6×10^7 s^{-1}).

For MHN21 on excitation at 320, 335, 350, and 360 nm, the lifetime modeling clearly yields two decay times of 0.34 and 1.22 ns. Several considerations are made in order to assign these decay times. As for the MHN21 molecule, there is also an excellent matching between both the excitation and the absorption spectra (Figure 3b). In addition, the equilibrium between N21-tautomer and NHB21 does not seem feasible in cyclohexane solution since the equilibrium constant has such a small value ($K = 3.6 \times 10^{-12}$, also estimated from the electronic energy in Table 1). An equilibrium constant of 9.0×10^{-3} for the rotamers N21-tautomer and HB21 and the IR data (cf. section 3) suggest that these two species are absorbing in the ground electronic state and contribute to the fluorescence spectra, though the ground state equilibrium is shifted to the former rotamer. The radiative lifetime (28.2 ns) estimated from the absorption spectra yields a radiative constant of 3.5×10^7 s^{-1}. The radiative constants ($K_f = \Phi_f/\tau_f$) calculated from the respective lifetimes and the fluorescence quantum yield ($\Phi_f =$ 0.04) are 3.3×10^7 s^{-1} (from 1.22 ns) and 1.2×10^8 s^{-1} (from 0.34 ns). As is observed, the radiative constant from the absorption spectrum matches the one corresponding to the lifetime of 1.22 ns, whereas the radiative constant corresponding to the 0.34 lifetime is larger by about 1 order of magnitude. On the grounds of the above reasonings we assign the 1.22 and 0.34 ns decay times to the N21-tautomer and HB21 isomers, respectively.

The decay time analysis for the short-wavelength emission of MHN23 in cyclohexane solution seems to be complex. In our measurements, we have employed a band-pass filter (Corion, LS-500- T−S226) in order to monitor only the short-wavelength fluorescence. The time-resolved analysis indicates that upon excitation either at 340, 360, or 380 nm, the phase modulation data reveal two decay times of 14.5 and 2.9 ns, with fractional contributions of 90% and 10%, respectively. That aforementioned evidence indicates the existence of several species in the S_1 state emitting within approximately the same spectral region. For the molecule MHN23 the electronic energy gap of NHB-1 with respect to HB or to N-tautomer is smaller than that between the corresponding tautomers of MHN12 and MHN21 (Table 1). In addition, there is an excellent matching between both the excitation spectra of the proton transfer emission and the absorption spectra of MHN23 (Figure 5), thereby meaning that the ground state chemical equilibria are shifted to the N23-tautomer. From our theoretical calculations, not only one but two nonintramolecular hydrogen bonded species could be present in the S_0 state (NHB23-1 and NHB23-2, Scheme 2) in view of the thermodynamic data, because the energy gap between them is only of 0.8 kcal/mol, NHB23-2 being the most stable conformer. However, the existence of NHB23-1 and NHB23-2 is not in accordance with the results gathered in Table 1, in which these two species lie at 11.5 and 10.7 kcal/mol higher than the N-tautomer. The calculated free energy values result in agreement with the respective electronic energy values given above. Since density functional calculations reproduce with great accuracy the experimental free energy of other ground state chemical reaction, as for example the ground state dimer-formation reaction of 7-azaindole (J. Catalán, to be published), the assignment of the lifetimes to the NHB23-1 and NHB23-2 is quite uncertained. NHB23-1 and NHB23-2 are stabilized in hydroxylic solvents by solute−solvent hydrogen bonding; therefore, their contribution must be much less important in cyclohexane solution. Thus, for MHN23 there are at least two absorbing species (N23-tautomer, HB23) in the ground electronic state that could fluoresce within the short wavelength emission band. On the other hand, from the absorption spectrum in cyclohexane a radiative constant (K_r) of 2.1×10^7 s^{-1} is calculated, which is several orders of magnitude larger than those radiative constants (K_f) estimated from the lifetimes and the fluorescence quantum yield (0.003), that is, 2.1×10^5 s^{-1} (from 14.5 ns) and 1.0×10^6 s^{-1} (from 2.9 ns). Thus, the photophysical data from the short-wavelength emission are not a consequence of the absorption spectrum and the main absorbing species (N23-tautomer). As a result, the N23-tautomer does not fluoresce within the short-wavelength band. At this stage, two possibilities can account for the ca. 98% of the N23-tautomer population generated in the S_1 state upon direct excitation: radiationless deactivation routes and the ESIPT mechanism (cf., Proton Transfer section). As we estimate below a proton transfer efficiency of 0.018, this process can be omitted as the main channel of deactivation of the N23-tautomer species.

In conclusion, the lifetime of 14.5 ns is ascribed to the HB23 tautomer based upon IR data, its large fractional contribution of emission (90%), and its radiative constant of 2.1×10^5 s^{-1}. Consequently, the lifetime of 2.9 ns could be tentatively assigned to a non-hydrogen bonded species (NHB). However, the species NHB23-1 and NHB23-2 do not seem to be feasible candidates. Aggregation effects can be precluded in these experiments because the solutions used were sufficiently diluted. More experiments are in progress in order to assign the 2.9 ns lifetime.

7. Photostability

The quantum yields of photoreaction under direct ultraviolet irradiation are for the first time reported for the molecules MHN12, MHN21, MS, and MHN23 in cyclohexane solution at 298 K (cf., Experimental section). Upon excitation at approximately the wavelength maxima (λ_{exc}) of the first absorption band, the following photoreaction quantum yields are obtained: 6.1×10^{-4} for MHN21 ($\lambda_{exc} = 340$ nm); 3.3×10^{-4} for MHN12 ($\lambda_{exc} = 340$ nm); 1.5×10^{-4} for MS ($\lambda_{exc} = 308$ nm); 2.7×10^{-5} for MHN23 ($\lambda_{exc} = 368$ nm). These quantum yields are as low as those reported for the archetype of photostability 2-(2′-hydroxy-5′-methylphenyl)benzotriazole (Tinuvin P).[7,34] All of the molecules above present strong intramolecular hydrogen bonds, but it is surprising that the molecule that contains the weakest one shows instead the highest photostability (cf., sections 8 and 9).

8. Gas-Phase Absorption and Emission

The gas-phase emission and absorption spectra (air equilibrated) of the molecules MHN12, MHN21, and MHN23 are depicted in Figures 6 and 7. The absorption spectra display slightly more vibronic structure and are blue shifted (ca. 550 cm^{-1} for MHN12, 450 cm^{-1} for MHN21, and 400 cm^{-1} for MHN23) in comparison to those obtained in cyclohexane solution. The red-shift dispersion found in cyclohexane solution compared to the gas phase is due to the well-known polarizability effect caused by the solvent.

Excitation of the molecules MHN12 and MHN21 in the gas phase gives rise to single fluorescence bands resembling those obtained in cyclohexane solution, but blue shifted and showing slightly less vibronic structure. It is important to highlight that their excitation spectra exhibit much smaller half widths than their respective gas-phase absorptions (Figure 7). This latter observation is made more evident for the gas phase at vacuum pressure conditions (degassed sample, without air), denoting that the absence of collisional relaxation produces the loss of a large part of the spectrum. These results are comparable to those reported[2] for methyl salicylate at the same experimental conditions, which were ascribed to the presence of an active radiationless channel.The above-mentioned evidence (Figure 7) demonstrates the presence of a radiationless deactivation channel in the hydrogen bonded N-tautomers of the molecules MHN12 and MHN21.

A dual fluorescence is shown in parts a and b of Figure 6 for MHN23, as is observed in cyclohexane solution, that is, the long-wavelength emission corresponding to the PT-tautomer and the short-wavelength emission arising from a mixture of emitting species (cf. section 6). Figures 7 and 8 display the effect of collisional relaxation on the long-wavelength and short-wavelength emissions, respectively, and denote the presence of radiationless deactivation pathways for the N23-tautomer and HB23. This radiationless deactivation pathways could be a feasible explanation, at least in part, for the high photostability demonstrated by MHN12, MHN21, and MHN23 in cyclohexane solution.

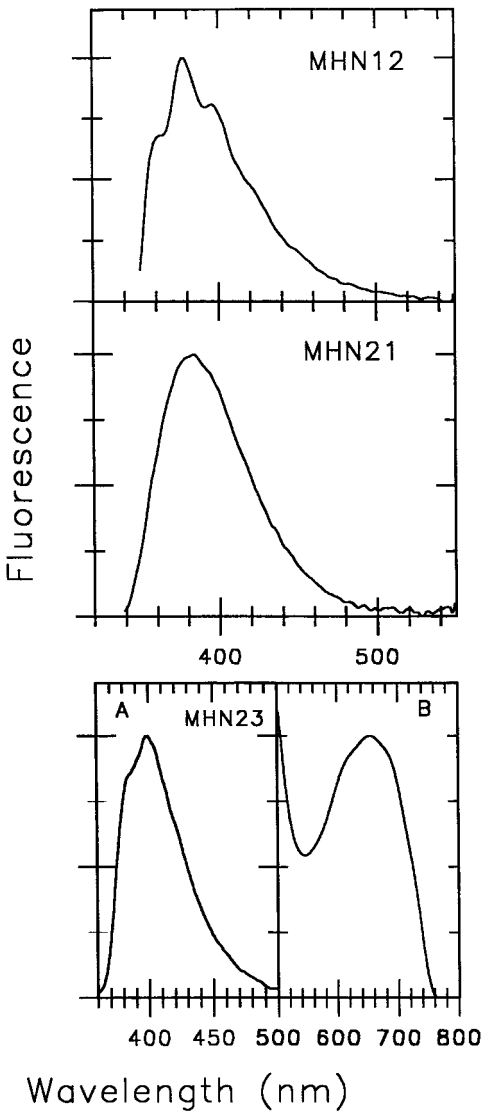

Figure 6. Gas-phase (air-equilibrated) fluorescence spectra at 353 K of the molecules MHN12, MHN21, and MHN23. A dual fluorescence is also observed for MHN23, the short-wavelength emission (A) and the proton transfer emission (B).

9. Proton Transfer

In this section we are concerned with two main points. On one hand, whether the ESIPT mechanism is responsible or not for the excellent photostability to direct ultraviolet irradiation exhibited by MHN23 in cyclohexane solution. On the other hand, we should explain the observation of ESIPT mechanism in the molecule MHN23 and its absence in MHN12 and MHN21.

Compounds containing an intramolecular hydrogen bond have hitherto received great attention for being very good photostabilizers because of their excellent photostability to ultraviolet irradiation. The 2-(2′-hydroxyphenyl)benzotriazoles, methyl salicylate and some of its derivatives exemplify this type of molecules. Since the compounds above present low PT-tautomer fluorescence quantum yields, some authors[2,4,7−9] have invoked the ESIPT mechanism to explain their great photostability. The photostability would rely on a rapid radiationless deactivation

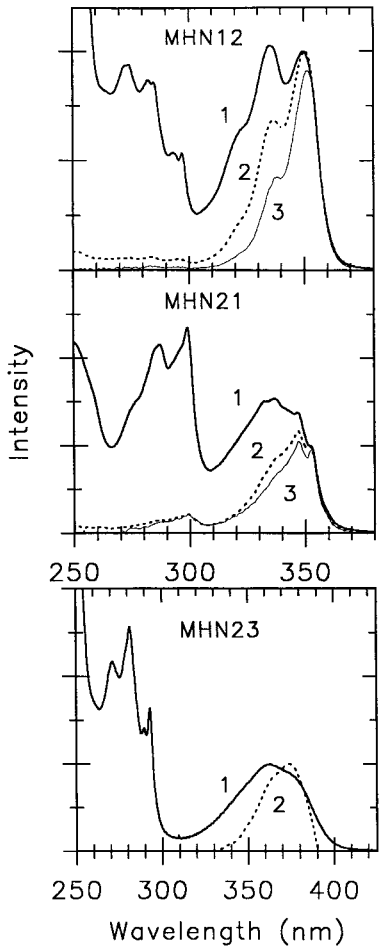

Figure 7. (1) Gas-phase (air-equilibrated) absorption spectra recorded using a 10 cm pathlength. (2) Gas-phase (air-equilibrated) excitation spectra of the compounds MHN12 and MHN21 and gas-phase (air equilibrated) excitation spectrum from the proton transfer emission of MHN23. (3) Gas-phase (without air, at a pressure of 4×10^{-5} mbar) excitation spectra of the molecules MHN12 and MHN21. All the spectra were measured at 353 K.

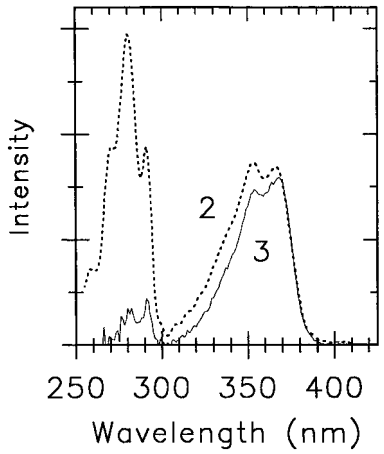

Figure 8. Gas-phase excitation spectra at 353 K from the short-wavelength emission of MHN23, (2) Air-equilibrated and (3) without air at a pressure of 4×10^{-5} mbar.

of the quinonoid form (PT-tautomer), which is caused by the approximation of the electronic states implicated in the intramolecular proton transfer emission.

The 2-(2′-hydroxyphenyl)benzotriazoles constitute a most important class of photoprotecting agents, for instance, the 5′-methyl derivative (2-(2′-hydroxy-5′-methylphenyl)benzotriazole, Tinuvin P) has been proposed as an archetype of photostability due to the photophysics of its PT-tautomer. However, the percentage of molecules transferring the proton in the excited state has been estimated for Tinuvin P to be very low (ca. 0.02%) in cyclohexane solution,[28] and experiments in dimethyl sulfoxide solutions show that its photostability is based upon avoiding the generation of non-hydrogen-bonded species,[30,34] which are in fact very reactive through the triplet state located at ca. 500 nm. These chemically reactive triplet states are quenched by another low lying triplet state at ca. 720 nm,[58] which corresponds to the chemical structures with a nonperturbed IMHB ring.

The molecules 3-hydroxyflavone,[24] salicylamide,[25] sodium salicylate,[26] and the 2-(*o*-hydroxyphenyl)benzimidazoles.[26,27] exhibit quite a distinct photophysical behavior compared to that of the 2-(2′-hydroxyphenyl)benzotriazoles. They present high proton transfer fluorescence quantum yields, and the ESIPT mechanism is recalled to explain their high gain coefficient values, since they are used as dye lasers.

Some other molecules as for example the phenylperimidines[35,36] and 1′-hydroxy-2′-acetonaphthone[32] present a strong intramolecular hydrogen bond, but do not yield an ESIPT mechanism, and they are even more photostable than Tinuvin P.

On the other hand, good photostabilizers, as for example the 2-hydroxybenzophenones and methylsalicylates, exhibit a high percentage of excited state proton transfer molecules. For instance, the methyl salicylate molecule has ca. 95% of the population[54] undergoing a proton phototransfer in cyclohexane solution. Therefore, the great photostability ($\Phi_r = 0.00015$) of methyl salicylate is definitely assignable to the photophysics of its PT-tautomer.

Therefore, it is a crucial point to estimate the percentage of MHN23 PT-tautomer species generated. Thus, the fluorescence quantum yield of the proton transfer tautomer is given by the following expression, $\Phi_F = \Phi_{TP}\Phi_F^C$, that is, the product of the proton transfer efficiency (Φ_{TP}) and the intrinsic fluorescence quantum yield of the PT-tautomer (Φ_F^C). As it is known, the quantum yield Φ_F^C is equal to the product $\tau_F^C k_F^C$, and since the PT-tautomer does not absorb in the ground state, the fluorescence radiative constant (k_F^C) must be estimated from lifetime (τ_F^C) measurements at low temperature, assuming it is independent of temperature. Therefore, the final expression for the proton transfer efficiency is given as follows, $\Phi_{TP} = [\Phi_F(\text{room temperature})\tau_F^C(\text{low temperature})]/\tau_F^C(\text{room temperature})$. From the literature (for degassed samples), the lifetimes at room temperature (at 298 K in methylcyclohexane) and low temperature (at 77 K in methylcyclohexane) are 0.23 and 0.59 ns,[10] respectively. Taking into account an intrinsic fluorescence quantum yield of 0.007,[10] the estimated percentage of MHN23 molecules evolving to the excited state PT-tautomer is as low as 1.8%. Thus, we can conclude that the great photostability ($\Phi_r = 0.000027$) shown by MHN23 in cyclohexane solution is not due to the photophysics of its PT-tautomer but to the photophysics of the N23-tautomer. For the sake of consistency, we have employed all the data from ref 10. However, there exist quantitative discrepancies of those data with ours. Our fluorescence quantum yields for MHN23 are much smaller than those given in ref 10. For instance, we have measured a proton transfer fluorescence quantum yield which is 10 times smaller than that given in ref 10. As for our measurements, all the fluorescence quantum yields have been measured 10 times, they being within a 15% stardard deviation. Also, the lifetime of the red emission from MHN23 was measured as 60 ps[1] vs a lifetime of 230 ps

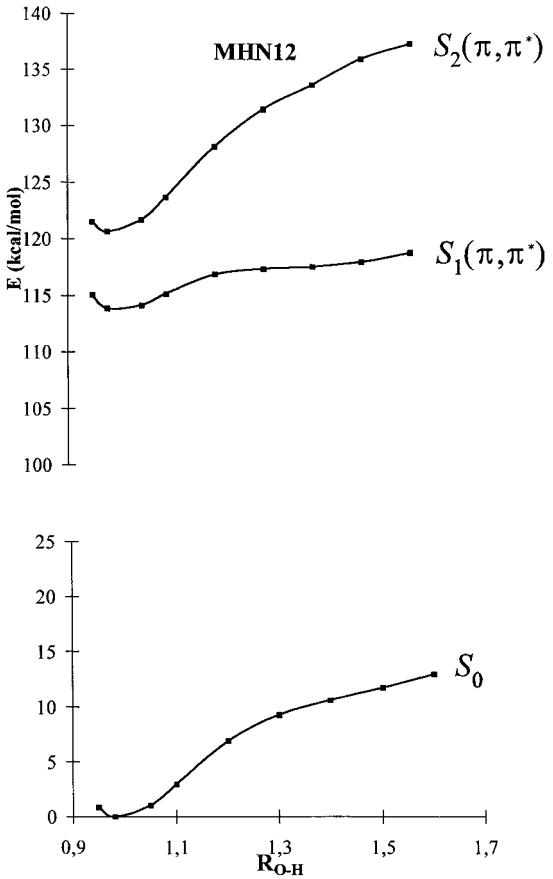

Figure 9. GSIPT curve (S_0), and ESIPT Franck−Condon curves of MHN12. The stretching O−H coordinate is given in angstroms.

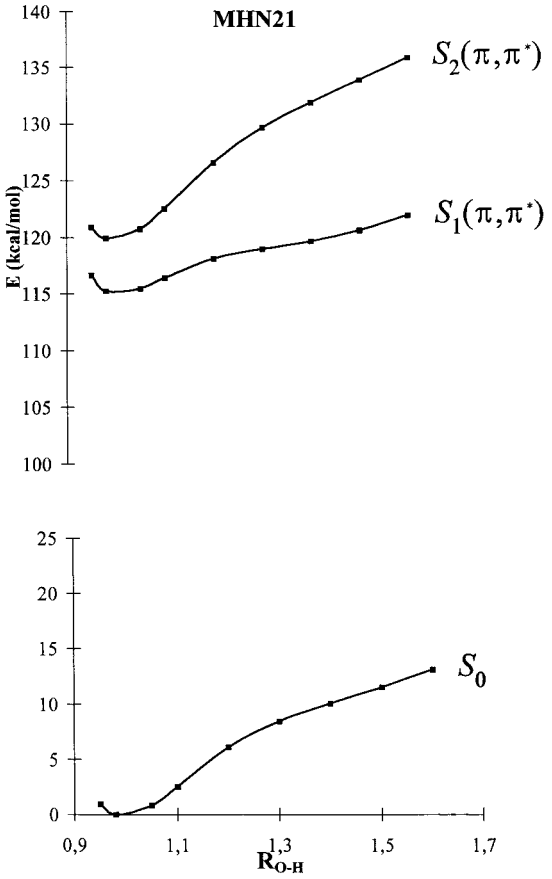

Figure 10. GSIPT curve (S_0) and ESIPT Franck−Condon curves of MHN21. The stretching O−H coordinate is given in angstroms.

reported in ref 10. However, the detection limit of our instrument ($\leq$30 ps) is much better than that given in ref 10 ($\leq$200 ps). Thus, if we take into account our data in conjunction with the 0.59 ns lifetime for the 77 K experiment from ref 10, a lower excited state proton transfer efficiency of 0.007 is obtained (0.7%).

Figures 9, 10, and 11 show the proton transfer potential energy curves either in the ground or excited states for the molecules MHN12, MHN21, and MHN23, respectively. As can be seen, the calculations at the level B3LYP/6-31G** provide ground state intramolecular proton transfer (GSIPT) curves with a single minimum at the equilibrium O−H distance of the N-tautomer. The GSIPT curves from the PT-tautomers are repulsive which implies that the proton transfer fluorescence does not show a vibronic structure, as is observed in Figures 4 and 6b for MHN23. The GSIPT curves for MHN12 and MHN21 are markedly stabilized with respect to that of MHN23 or MS.[48] This markedly stabilized GSIPT curve for the proton transferred form, also found for the molecule 1-hydroxy-2-acetonaphthone, was explained as a result of the higher polarizability of the naphthalene residue.[46] Thus, this polarizability interaction might be approximately the same for the three naphthalene type compounds. However, the ground state energy increment value (cf., Experimental section, E_{PT}, Table 1) for the molecule MHN23 (21.5 kcal/mol) is much larger than that of MHN12 (13.1 kcal/mol) and MHN21 (13.0 kcal/mol).

The differences of relative E_{PT} values of MHN21, MHN12, and MHN23 with respect to MS cannot be rationalized due to structural constraints, since all of them undergo similar bond distance changes because of the proton tranfer process and possess the characteristic hydrogen bond distances $O_1\cdots O_{5'}$ and $O_{5'}\cdots H$ (Table 2).

The $1(\pi,\pi^*)^1$ potential energy curves of MHN12 and MHN21 exhibit a single minimum at the equilibrium distance of the N-tautomer and therefore intramolecular proton transfer is hindered. Instead of that, MHN23 presents a $1(\pi,\pi^*)^1$ state with double-well, and an exothermal behavior of the potential curve of the PT-tautomer, which explains the occurrence of the proton transfer fluorescence observed in cyclohexane solution. The calculations suggest that enol−keto (N-tautomer → PT-tautomer) tautomerization is completed after ESIPT. The calculated energy barrier for the ESIPT process of MHN23 is around 1.5 kcal/mol. We can conclude from the aforementioned theoretical data that the ESIPT mechanism is only energetically favorable in the molecule MHN23. The existence of two potential energy wells could enable the existence of two fluorescences, that is, from the N23-tautomer and the PT-tautomer (both corresponding to hydrogen bonded species), but the former emission has not been detected (cf. section 6).

A decisive insight on the different profiles of the GSIPT and ESIPT curves can be acquired by analyzing the ground-state molecular orbitals HOMO and LUMO (Figures 12, 13, and 14) along the proton-transfer coordinate of the molecules studied. The HOMO−LUMO transition chiefly[59] describes the first singlet excited states of all the molecules studied, in other words, the $[1(\pi,\pi^*)^1]$ state is characterized by exciting one electron from the π HOMO (highest occupied molecular orbital) to the π^* LUMO (lowest unoccupied molecular orbital). Both HOMO and LUMO are of π-type, however their phases are not equal for the molecules MHN12, MHN21, and MHN23. Indeed, the HOMO orbital of the N12-tautomer correlates with the highest occupied π orbital of 1-naphthol, and the HOMO orbitals of N21-tautomer and N23-tautomer correlate with that of 2-naphthol.[60] The HOMO orbital on the IMHB system of MHN12

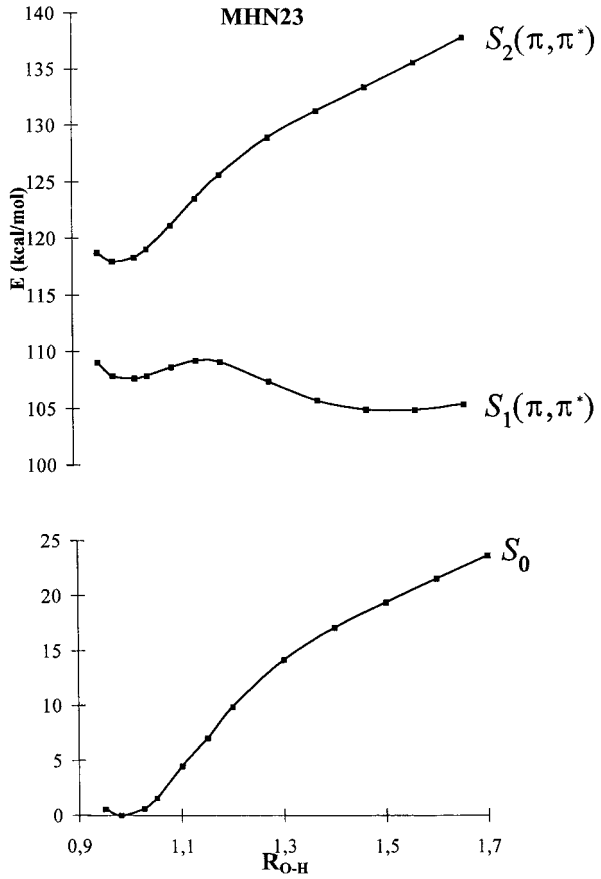

Figure 11. GSIPT curve (S_0) and ESIPT Franck−Condon curves of MHN23. The stretching O−H coordinate is given in angstroms.

(Figure 12) is primarily of $C_{2'}C_{3'}[C_{4'}]$ bonding character, in addition to the $C_{2'}O_{1'}$ and $C_{4'}O_{5'}$ antibonding contribution. Both oxygen atoms have a bonding character, with a larger HOMO projection over the hydroxyl oxygen ($O_{1'}$). For MHN12 (Figure 12), the electronic rearrangements induced by ground state proton transfer lead to an HOMO projection still very large over the $O_{1'}$ atom, and also shifted to the $C_{3'}-C_{4'}$ bond. As is shown in Figure 13, the MHN21 compound has an HOMO projection on the IMHB system with similar characteristics to that of HOMO orbital of MHN12 (Figure 12). In contrast, HOMO is distinctly projected on the IMHB system of MHN23 (Figure 14), principally because of the existence of a node at position 3 of the naphthalene ring ($C_{3'}$, Scheme 1), as it is found for the 2-naphthol HOMO orbital.[60] Furthermore, there is no electronic density contribution over the ester group of MHN23. Proton transfer in the ground state produces an HOMO orbital of MHN23 with less electronic density projection over $C_{3'}-C_{4'}$ and $O_{5'}$ than that of the HOMO orbital of the molecules MHN12 and MHN21.

In conclusion, for the ground state of MHN23, the lower conjugation through the IMHB system and the lower basicity of carbonyl group weakens its IMHB strength, that together with a less effective electronic transfer along the proton transfer coordinate make the GSIPT process nonviable. The opposite effects are found for the MHN12 and MHN21 molecules, thereby strengthening the IMHB system and stabilizing the GSIPT potential energy curves with respect to that of MS. Nevertheless, this stabilization is not sufficient for producing a GSIPT process.

On the other hand, the LUMO is a π^* orbital for the three compounds studied that also presents $C_{2'}O_{1'}$ and $C_{4'}O_{5'}$ antibonding character, as the HOMO electronic map, but with a $C_{3'}C_{4'}$ bonding character and some $C_{2'}C_{3'}$ antibonding contribution on the IMHB system (Figures 12−14). Weighty differences are also found between MHN23, and both MHN12 and MHN21. The LUMO orbital of N23-tautomer (Figure 14) possesses a high projection on the $O_{5'}$ atom and a null projection on the $O_{1'}$ atom (in the opposite way to the HOMO), whereas for MHN12 (Figure 12) and MHN21 (Figure 13), the LUMO orbital presents slightly higher projection on the $O_{5'}$ atom and lower projection on $O_{1'}$ than that for the respective oxygen atoms of the HOMO orbital. After tautomerization, the LUMO orbital of the PT-tautomer of MHN23 still exhibits a large electronic density projection on the $O_{5'}$ atom, and almost null projection on the $O_{1'}$ atom, thereby favoring the proton transfer process. In

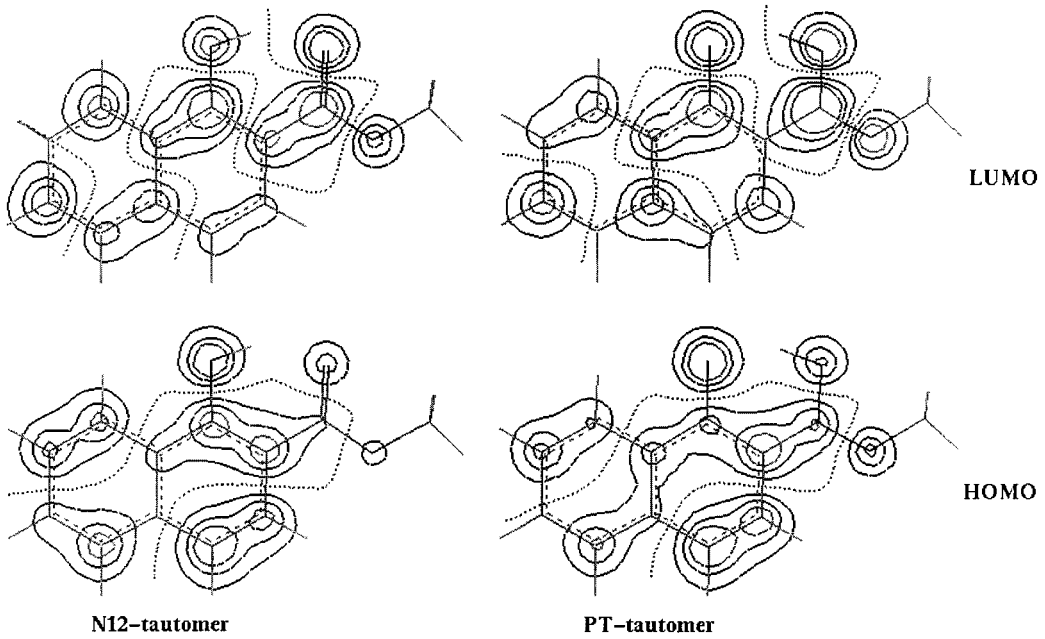

Figure 12. Two-dimensional plots of the HOMO and LUMO orbitals, which are involved in the electronic excitation from S_0 to S_1 of the N-tautomer and the PT-tautomer (R_{O-H} = 1.6 Å) of MHN12. The HOMO and LUMO drawings are evaluated 0.3 Å above the molecular plane. The nodal planes are represented by dashed lines, and the contour lines are drawn every 0.03 au.

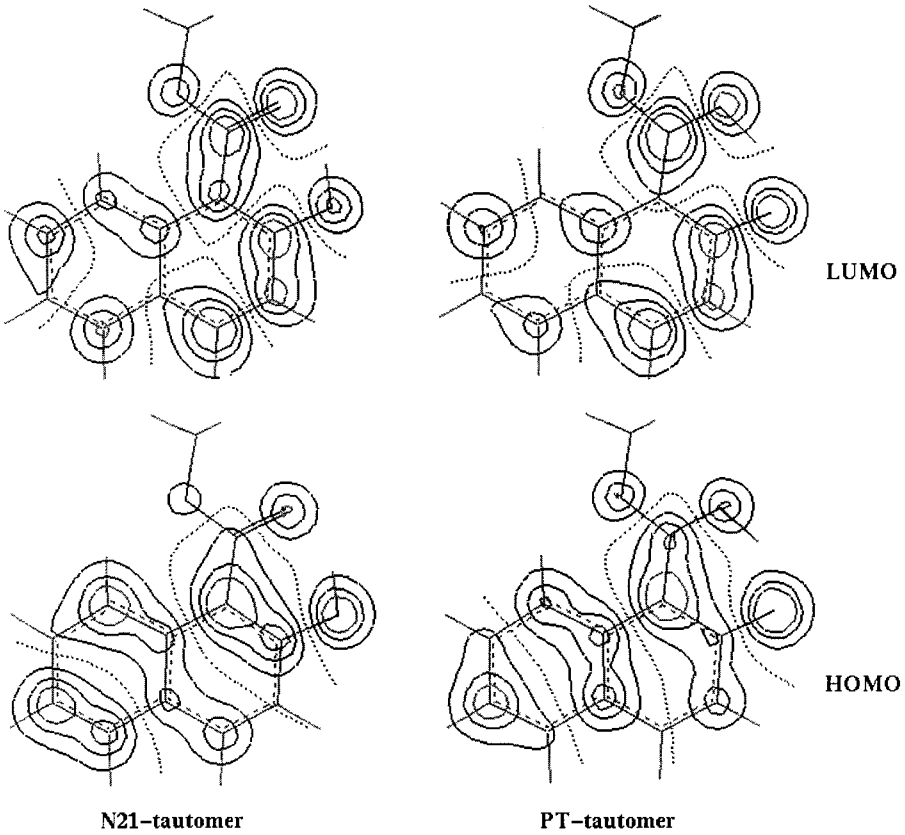

Figure 13. Two-dimensional plots of the HOMO and LUMO orbitals, which are involved in the electronic excitation from S_0 to S_1 of the N-tautomer and the PT-tautomer (R_{O-H} = 1.6 Å) of MHN21. The HOMO and LUMO drawings are evaluated 0.3 Å above the molecular plane. The nodal planes are represented by dashed lines, and the contour lines are drawn every 0.03 au.

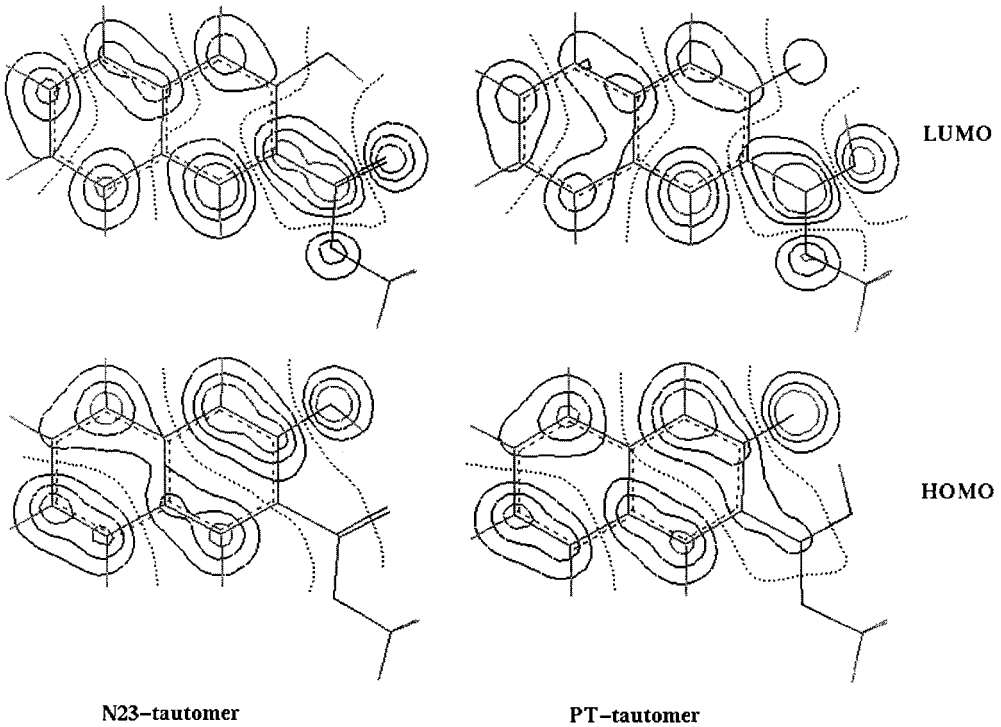

Figure 14. Two-dimensional plots of the HOMO and LUMO orbitals, which are involved in the electronic excitation from S_0 to S_1 of the N-tautomer and the PT-tautomer (R_{O-H} = 1.6 Å) of MHN23. The HOMO and LUMO drawings are evaluated 0.3 Å above the molecular plane. The nodal planes are represented by dashed lines, and the contour lines are drawn every 0.03 au.

contrast, for the proton-transfer process of MHN12 and MHN21, the LUMO orbital still shows a large electronic density projection on the $O_{1'}$ atom, and thus the proton transfer is strongly hindered.

To sum up, the ESIPT process is driven from the N-tautomer to the PT-tautomer of MHN23 because of the drastic changes in acidity and basicity shown by the functional groups upon excitation and the associated changes in electrostatic attraction

of the bridging hydrogen. Since this latter evidence is absent for the S_1 state of MHN12 and MHN21, an ESIPT mechanism is precluded for these molecules.

Also, we should call attention to the fact that for the three molecular systems studied the second excited singlet electronic state $[2(\pi,\pi^*)^1]$ does not go through a proton transfer process (Figures 9−11). This evidence is being currently tested in our laboratory.

10. Conclusions

The photophysical, IR, and theoretical data reveal that the compounds studied possess predominant absorbing hydrogen bonded N-tautomer species in the ground electronic state. The intramolecular hydrogen bond strength for the N-tautomers according to IR and theoretical data is on the decrease for the following molecular sequence MHN21, MHN12, and MHN23. Though MHN23 presents the weakest intramolecular hydrogen bond, upon excitation it is definitely the only molecule which undergoes an ESIPT mechanism. For the molecules MHN12, MHN21, and MHN23, the relative position of the intramolecular hydrogen bond on the naphthalene ring (i.e., the 1−2, 2−1, and 2−3 linkings) determines both its strength and the occurrence of an ESIPT mechanism. The intramolecular hydrogen bond strength is, on one hand, explained by the conjugation of the IMHB ring with the naphthalene ring; thus, the stronger conjugation the greater the IMHB strength is. As is theoretically demonstrated, the electronic density distributions indicate an IMHB ring, which is much more conjugated with the naphthalene ring for the molecules MHN12 and MHN21 than for MHN23. On the other hand, the position of the IMHB in the molecular skeleton influences greatly the electronic transfer produced upon excitation between the carbonyl and hydroxyl groups (involved in the intramolecular hydrogen bond), which increases their basicity and acidity, respectively, thereby favoring the ESIPT mechanism for the molecule MHN23. In contrast, no evidence of such definite electronic transfer within the IMHB ring is shown by the molecules MHN12 and MHN21.

All the molecules studied exhibit a great photostability to direct ultraviolet irradiation, comparable to the photostability exhibited by some of the most renowned standards (e.g., methyl salicylate and Tinuvin P). Furthermore, the quantum yield of photoreaction of MHN23 is times smaller than that of the molecules MHN12, MHN21, and methylsalicylate. The low $S_1 \rightarrow S_1'$ excited state proton transfer efficiency of 0.018 discards the ESIPT mechanism as the principal cause of photostability for the molecule MHN23. As a result, the great photostability of MHN23 does not rely on the photophysics of the PT-tautomer but on the photophysics of the N23-tautomer. Nonradiative mechanisms of the N23-tautomer are to be studied. The triplet state photophysics may have an important role on this point, and thus data on intersystem crossing (ISC) yields would be important to understand the deactivation pathways in these molecules. Also, for MHN23, an ESIPT process from the triplet state manifold offers a new pathway which remains under research.

Acknowledgment. We are greatly indebted to DGICYT of Spain (Project PB93-0280) for financial support. One of us (J.P.) acknowledges with thanks the granting of an F.P.I. scholarship by the Ministry of Education and Science of Spain. C. Díaz acknowledges Comunidad Autónoma de Madrid for a postdoctoral fellowship. We are also grateful to Centro de Computación Cientifica de la Facultad de Ciencias (CCCFC) for CPU facilities.

References and Notes

(1) Woolfe, G. J.; Thistlethwaite, P. J. *J. Am. Chem. Soc*. **1981**, *103*, 3949.
(2) Acuña, A. U.; Catalán, J.; Toribio, F. *J. Phys. Chem*. **1981**, *85*, 241.
(3) Heller, H. J. *Eur. Polym. J. Suppl*. **1969**, 105.
(4) Williams, D. L.; Heller, A. *J. Phys. Chem.* **1970**, *74*, 4473.
(5) Heller, H. J.; Blattman, H. R. *Pure Appl. Chem.* **1972**, *30*, 145.
(6) Heller, H. J.; Blattman, H. R. *Pure Appl. Chem*. **1973**, *36*, 141.
(7) Otterstedt, J. E. A. *J. Phys. Chem.* **1973**, *58*, 5716.
(8) Klöpffer, W. In *Advances in Photochemistry*; Pitts, F. J. N., Jr., Hammond, S. S., Gollnick, K., Eds.; Wiley: New York, 1977; Vol. 10, p 311 and references therein.
(9) Werner, T. *J. Phys. Chem.* **1979**, *83*, 320.
(10) Law, K.-Y.; Shoham, J. *J. Phys. Chem*., **1994**, *98*, 3114.
(11) Tobita, S.; Yamamoto, M.; Kurahayashi, N.; Tsukagoshi, R.; Nakamura, Y.; Shizuka, H. *J. Phys. Chem. A* **1998**, *102*, 5206.
(12) Bergmann, E. D.; Hirshberg, Y.; Pinchas, S. *J. Chem. Soc.*, **1950**, 2351.
(13) Naboikin, U. V.; Zadorozhnyi, B. A.; Pavlova, E. N. *Opt. Spectrosc.* (Eng. Transl.) **1959**, *6*, 312.
(14) Weller, A. *Naturwiss.* **1955**, *42*, 175.
(15) Weller, A. *Zs. Elektrochem.* **1956**, 60 (*9*), 1144.
(16) Weller, A. *Prog. React. Kinet.* **1961**, *1*, 189.
(17) Woolfe, G. J.; Thistlethwaite, P. J. *J. Am. Chem. Soc*. **1980**, *102*, 6917.
(18) Nomura, Y.; Ide, N.; Ohtaki, K.; Tomita, M.; Tosaka, H.; Nanya, T.; Orihara, M.; Chiba, S.; Inoue, S.; Asahina, Y.; Fushimi, H. U.S. Patent 4,762,763, 1988.
(19) Kawagishi, Y.; Narita, S.; Kiriu, T.; Uomoto, K. U.S. Patent 4,656,112, 1987.
(20) Kiriu, T.; Arakawa, M. U.S. Patent 4,845,003, 1985.
(21) Kiuchi, T.; Maki, I. U.S. Patent 4,206,064, 1980.
(22) Hashimoto, K.; Maruta, M.; Soyama, H.; Ishii, Y. U.S. Patent 4,767,688, 1988.
(23) Khan, A. U.; Kasha, M. *Proc. Natl. Acad. Sci. U.S.A.* **1983**, *80*, 1767.
(24) Chou, P.; McMorrow, D.; Aartsma, T. J.; Kasha, M. *J. Phys. Chem.* **1984**, *88*, 4596.
(25) Acuña, A. U.; Costela, A.; Muñoz, J. M. *J. Phys. Chem.* **1986**, *90*, 2807.
(26) Acuña, A. U.; Amat, F.; Catalán, J.; Costela, A.; Figuera, J. M.; Muñoz, J. M. *Chem. Phys. Lett.* **1986**, *132* (6), 567.
(27) Costela, A.; Amat, F.; Catalán, J.; Douhal, A.; Figuera, J. M.; Muñoz, J. M.; Acuña, A. U. *Opt. Commun.* **1987**, *64* (5), 459.
(28) Catalán, J.; Fabero, F.; Guijarro M. S.; Claramunt, R. M.; Santa María, M. D.; Foces-Foces, M. C.; Hernández-Cano, F.; Elguero, J.; Sastre, R. *J. Am. Chem. Soc.* **1990**, *112*, 747.
(29) Sastre, R.; Catalina, F.; Mateo, J. L.; Claramunt, R. M.; Santa María, M. D.; Catalán, J. *J. Polym. Sci.: Polym. Chem*. **1990**, *28*, 3661.
(30) Catalán, J.; Pérez, P.; Fabero, F.; Wilshire, J. F. K.; Claramunt, R. M.; Elguero, J. *J. Am. Chem. Soc*. **1992**, *114*, 964.
(31) Catalán, J.; Fabero, F.; Claramunt, R. M.; Santa María, M. D.; Foces-Foces, M. C.; Hernández-Cano, F.; Martínez-Ripoll, M.; Elguero, J.; Sastre, R. *J. Am. Chem. Soc.* **1992**, *114*, 5039.
(32) Catalán, J.; del Valle, J. C. *J. Am. Chem. Soc*. **1993**, *115*, 4321.
(33) Catalán, J.; del Valle, J. C.; Claramunt, R. M.; Santa María, M. D.; Bobosik, V.; Mocelo, R.; Elguero, J. *J. Org. Chem*. **1995**, *60*, 3427.
(34) Catalán, J.; del Valle, J. C.; Fabero, F.; García, N. *Photochem. Photobiol*. **1995**, *61*, 118.
(35) Catalán, J.; del Valle, J. C.; Claramunt, R. M.; Sanz, D.; Dotor, J. *J. Lumin.* **1996**, *68*, 165.
(36) del Valle, J. C.; Catalán, J.; Foces-Foces, M. C.; Llamas-Saiz, A. L.; Elguero, J.; Sanz, D.; Dotor, J.; Claramunt, R. M. *J. Lumin.* **1997**, *75*, 17.
(37) Catalán, J.; de Paz, J. L. G.; Torres, M. R.; Tornero, J. D. *J. Chem. Soc., Faraday Trans.* **1997**, *93*, 1691.
(38) Heller, H. G.; Langan, J. R. *J. Chem. Soc., Perkin Trans. 2*, **1981**, 341.
(39) Barone, V.; Adamo, C. *Int. J. Quantum Chem.* **1997**, *61*, 429.
(40) Barone, V.; Adamo, C. *J. Chem. Phys.* **1996**, *105*, 11007.
(41) Lampert, H.; Mikenda, W.; Karpfen, A. *J. Phys. Chem.* **1997**, *100*, 22254.
(42) Hass, K. C.; Schemeider, W. F.; Estévez, C. M.; Bach, R. D. *Chem. Phys. Lett.* **1996**, *263*, 414.
(43) Becke, A. D. *J. Chem. Phys.* **1993**, *98*, 5648.
(44) Lee, C.; Yang, W.; Parr, R. G. *Phys. Rev.* **1988**, *B37*, 785.
(45) Wong, M. W. *Chem. Phys. Lett.* **1996**, *256*, 391.
(46) Catalán, J.; Palomar, J.; De Paz, J. L. G. *Chem. Phys. Lett.* **1997**, *269*, 151.
(47) Foresman, J. B.; Head-Gordon, M.; Pople, J. A. *J. Phys. Chem*. **1992**, *96*, 135.

(48) Catalán, J.; Palomar, J.; De Paz, J. L. G. *J. Phys. Chem. A* **1997**, *101*, 7914.
(49) Frisch, M. J.; Trucks, G. W.; Head-Gordon, M.; Gill, P.; Wong, M. W.; Foresman, J. B.; Johnson, B. J.; Schlegel, H. B.; Robb, M. A.; Repogle, E. S.; Gomperts, R.; André, J. L.; Raghavachari, K.; Binkley, J. S.; Gonzalez, C.; Martin, R. L.; Fox, D. J.; Defrees, D. J.; Baker, J.; Stewart, J. P.; Pople, J. A. *Gaussian 94*, revision D.1; Gaussian Inc.: Pittsburgh PA, 1996.
(50) Gilli, G.; Belluci, F.; Ferreti, V.; Bertolasi, V. *J. Am. Chem. Soc.* **1989**, *111*, 1023.
(51) Hunsberger, I. M. *J. Am. Chem. Soc*. **1950**, *72*, 5626.
(52) Porte, A. L.; Gutowsky, H. S.; Hunsberger, I. M. *J. Am. Chem. Soc*. **1960**, *82*, 5057.
(53) Zadorohnyi, B. A.; Ischenko, I. K. *Opt. Spectrosc*. **1965**, *19*, 306.
(54) Toribio, F.; Catalán, J.; Amat-Guerri, F.; Acuña, A. U. *J. Phys. Chem.* **1983**, *87*, 817.
(55) Berlman, I. D. *Handbook of Fluorescence Spectra of Aromatic Molecules*; Academic: New York, 1965.
(56) Platt, J. R. *J. Chem. Phys.* **1949**, *17*, 484.
(57) Strickler, S. J.; Berg, R. A. *J. Chem. Phys.* **1962**, *37*, 814.
(58) Catalán, J. *Chem. Phys. Lett*. **1998**, *297*, 549 and results to be published.
(59) The $HOMO^{-1} \rightarrow LUMO^{+1}$ excitation represents the second major contribution (ca. 15%) for all of the S_1 transitions of the molecules studied, except for the one corresponding to the PT-tautomer of MHN23, which is described exclusively as an HOMO → LUMO excitation.
(60) Utsunomiya, C.; Kobayashi, T. Nagakura, S. *Bull. Chem. Soc. Jpn.* **1975**, *86*, 1852.